Physica B 167 (1990) 247–256
North-Holland

THE STRUCTURE OF a-$Si_{1-x}Sn_x$:H THIN FILMS

A.M. EDWARDS, M.C. FAIRBANKS and R.J. NEWPORT
Physics Laboratory, University of Kent, Canterbury CT2 7NR, UK

Received 11 May 1990

The doping of a-Si:H with Sn is known to modify the electrical and optical properties of the material. The optical band gap decreases as the doping level is increased, however, there is no insulator–metal transition of the type observed, for example, when transition metals are used as dopants. In order to increase the understanding of the conductivity processes that occur in a-Si:metal:H alloys we have measured the atomic scale structure of a series of a-$Si_{1-x}Sn_x$:H thin-films using EXAFS. Samples were prepared by RF reactive co-sputtering and both Si and Sn K-edge EXAFS examined. The results indicate that the Sn atoms are substituted randomly into the a-Si tetrahedral random network. Both Si and Sn atoms retain fourfold co-ordination over the composition range studied ($0 \leq x \leq 0.18$). In contrast to results obtained using transition metal dopants there is no local modification of the tetrahedral random network.

1. Introduction

Previous reports on the structure of a-Si:Ni:H [1] and a-Ge:Mo [2] thin films have shown that incorporation of a transition metal leads to modifications of the tetrahedral structure of the amorphous semiconductor to yield local atomic arrangements similar to those observed in intermetallic compounds. There appears to be no substitution of metal atoms for semiconductor atoms in the tetrahedral random network (TRN) and the metal atoms do not occupy interstitial sites, rather the metal-modified regions coexist with the remaining semiconductor TRN. The primary motivation for interest in this type of system is the understanding the structural changes that accompany the occurrence of an insulator–metal transition (MIT) as the proportion of metal in the material is increased.

Another semiconductor–metal system of great interest may be formed by alloying tin with hydrogenated amorphous silicon (a-$Si_{1-x}Sn_x$:H). In contrast to the transition metal systems discussed above this alloy does not exhibit an MIT. As the proportion of Sn is increased the optical band gap, E_0, is known to decrease monotonically [3, 4]. However, the dark DC conductivity has been found to increase less than would be expected on the basis of a conduction mechanism with an activation energy close to one half of the optical gap [3, 5, 6]. Indeed, the dark conductivity has been found by some workers to show a minimum at an optical gap corresponding to a value of ~1.7 eV [7, 8] indicating a change from n- to p-type conduction at the corresponding Sn concentration (<5 at%). This change of carrier type has been interpreted as indicating the inclusion of Sn atoms as interstitial impurities rather than substitutionally and results in a loss of photoconductivity and poor performance in solar cells. The suppressed increase of DC dark conductivity, along with its temperature dependence, lead all these authors [3–8] to the conclusion that the conduction mechanism changes from extended state to localized state hopping. Despite these extensive optical and electronic studies, less attention has been focussed on the structural variation of a-Si:Sn(:H) with increasing Sn content; although some structural conclusions have been drawn from infrared spectroscopy [3, 5], and limited electron [9] and X-ray [10, 11] diffraction; while the Sn sites have been probed by ^{119}Sn Mössbauer spectroscopy [5, 9]. However, many of these studies have centred on unhydrogenated, evaporated samples, which may not be representative of the device quality hydrogenated material prepared by plasma deposition methods. In

0921-4526/90/$03.50 © 1990 – Elsevier Science Publishers B.V. (North-Holland)

order to clarify the causes of the electronic and optical properties of this alloy system a detailed understanding of the atomic scale structure is necessary. Hence, we have investigated both the Si and Sn local environments in a series of sputtered alloys using the chemical specific EXAFS technique.

2. Sample preparation and characterisation

RF reactive co-sputtering [12] was used to deposit a series of thin film samples of a-$Si_{1-x}Sn_x$:H onto the variety of uncooled substrates necessary for complete sample characterisation. The preparation conditions used for differing compositions were held constant, the RF power used was 200 W, the target substrate distance was 5.5 cm and the total sputtering pressure was 7.3×10^{-3} mbar. The sputtering gas used was an argon/hydrogen mixture in the ratio 10:1; the hydrogen is used to saturate any dangling bonds that may occur and is known to improve substantially the electronic characteristics of the material. The composition of the thin films was controlled by varying the number of small discs of tin placed on the crystalline silicon sputtering target. These discs were arranged to produce a macroscopically homogeneous sample and this was later checked using SEM. Neither SAED–TEM nor SEM measurements indicated clusters of metallic (β-Sn or any other form of crystallinity in any of the films. Sample compositions were determined using energy dispersive electron microprobe analysis and $^4He^+$ Rutherford backscattering. Immediately after deposition all of the films were found to contain approximately 8 at% Ar, although desorption of Ar was found to occur with time.

IR spectra for a-Si:Sn:H are shown in fig. 1 for the wave number range 1500–2500 cm^{-1}. There appears to be no systematic shift in wave number nor variation in intensity with increasing Sn. This latter fact suggests that the number of Si–H bonds is not altered appreciably in this concentration range. The most important aspect of these spectra is the lack of any Sn–H features, expected ~1700–2000 cm^{-1} [3, 5, 6, 8]. However, this may be due to a strong preference of the hydrogen to bond to the Si rather than the Sn in the absence of sufficient H_2 to saturate all the dangling bonds in the system. A preference ratio of up to 12:1 for Si–H bonds compared to Sn–H bonds has been reported by Von Roedern et al. [8]. This technique was also used to verify that the films were not contaminated with significant amounts of either oxygen or nitrogen.

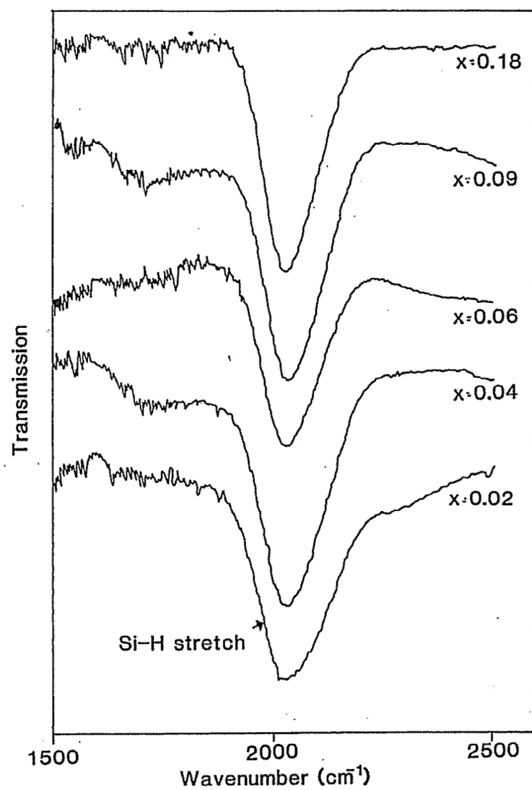

Fig. 1. IR absorption spectra of some a-$Si_{1-x}Sn_x$:H samples (spectra vertically offset for clarity).

Initial DC dark conductivity measurements on the films prepared for this study were performed in a parallel study at the University of Leicester [13]. These appeared to show $T^{-1/4}$ dependence below room temperature, indicative of variable range hopping, and T^{-1} dependent localized state conduction for the majority of samples above room temperature. This is in qualitative agreement with the results of Maloufi et al. [14]. The dependence of room temperature dark conductivity on Sn concentration showed good qual-

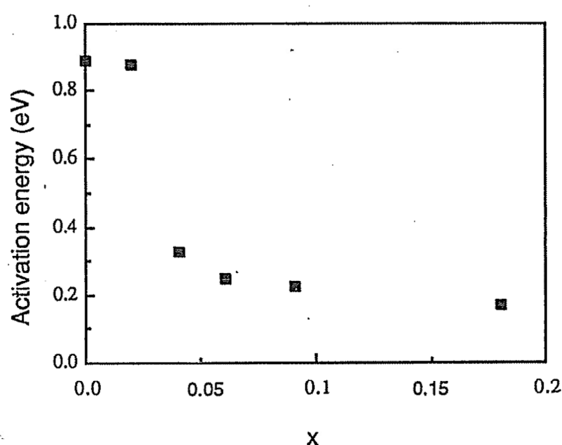

Fig. 2. Variation of activation energy with Sn content for a-$Si_{1-x}Sn_x$:H.

itative agreement with that of Girginoudi et al. [6], as did the variation of activation energy with x (fig. 2 [13]). From this figure, the 0.9 eV activation energy (typical for undoped a-Si:H alloys) indicates that for values of x up to ~0.03, the conduction mechanism is of free carrier type. A transition from extended to localized state conduction, and a correspondingly large decrease in activation energy to around 0.2 eV (typical for heavily doped a-Si:H alloys) appears to occur above this metal concentration. In addition, relatively low crystallization temperatures were discovered for all films; between ~140 and 170°C, decreasing with increasing Sn content.

3. Experimental

Extended X-ray absorption fine structure (EXAFS) data at both the Si and Sn K-edges were collected at the 2 GeV Synchrotron Radiation Source (SRS) at the Daresbury Laboratory.

Si K-edge spectra were measured on the soft X-ray beamline 3.4. Monochromation of the incident X-ray beam was achieved using an InSb double crystal monochromator, allowing rejection of higher order harmonics. The intensity of the incident beam was monitored using an Al foil and absorption at the thin film sample was measured using the electron drain current method, a variation on the electron total yield technique [15]. Samples used in this series of experiments were deposited to a thickness of approximately 2 μm on stainless steel substrates.

Sn K-edge experiments were performed on the hard X-ray (wiggler) beamline using station 9.2. At the time of use this instrument was fitted with a Si (2 2 0) double crystal monochromator. Unfortunately, at the Sn K-edge this monochromator is at the limit of its useful range, producing only low intensity. The experiments were performed in a standard transmission configuration, the beam intensity being measured with Kr/He gas ionisation detectors. Samples used in these experiments were deposited on thin (~0.02 mm) sheets of polypropylene and stacked to provide, as near as possible, the optimum increase ($\Delta\mu = 1.5$) in absorption at the K-edge.

More comprehensive descriptions of the beamlines used can be found elsewhere [16].

4. Data analysis

Background subtraction and normalisation of the experimental data was performed in the normal way using the program EXBACK [17] available at the SRS. The edge position was chosen to occur at the position of the principal maximum in the first derivative of the raw data. Pre- ($\mu_0(k)$) and post-edge ($\mu(k)$) backgrounds were calculated by fitting smooth, low-order polynomials to the appropriate regions of the experimental spectra. Normalization was then performed to yield the EXAFS function, $\chi(k)$, as shown in eq. (1):

$$\chi(k) = \frac{\mu(k) - \mu_0(k)}{\mu_0(k)} . \quad (1)$$

As an illustration of the information contained in EXAFS, eq. (2) shows a simplified expression for $\chi(k)$ in terms of the structural parameters of the absorbing medium:

$$\chi(k) = \sum_{i=1}^{n} \frac{N_i AFAC}{kR_i^2} |F_i(\pi, k)| \exp(-A_i k^2) \times \exp(-2R_i/\lambda) \sin(2kR_i + 2\delta + \psi_i) . \quad (2)$$

Here N_i is the number of neighbouring atoms in

a shell of radius R_i around the central (absorbing) atom. Each of these atoms backscatters the emitted photoelectron with an amplitude $F_i(\pi, k)$. The exponential containing A_i is an effective Debye–Waller factor which provides a description of the static and thermal disorder in the system. The coefficient $A_i = 2\sigma_i^2$ where σ_i is the root mean square deviation in interatomic distances R_i (this assumes a Gaussian distribution of interatomic distances). The second exponential term in eq. (2) accounts for losses caused by inelastic scattering of the photoelectron, λ being the electron mean free path which is usually described in terms of an imaginary potential (VPI). The sine term in the equation accounts for phase shifts experienced by the photoelectron on passing through the emitting atom potential (δ) and during backscattering (ψ_i). The term AFAC accounts for events that result in absorption except EXAFS, such as multiple electron excitations. A further, non-structural parameter that needs to be included is E_0, the magnitude of the photoelectron energy at zero wave vector ($k = 0$).

Evaluation of parameters E_0, R, N, A and VPI from the experimental results was achieved by non-linear least squares fitting of the rapid curved wave theory of EXAFS [18] using the interactive package EXCURV88 [19]. The term AFAC was always fixed by reference to a standard sample with the same central atom. The backscattering factor and phase shifts were calculated within EXCURV88 and modified empirically if necessary so that the known structural parameters for the standard compounds, crystalline Si and metallic Sn, were reproduced to within the experimental error.

Experimental errors and the possible significance of increasing the number of atomic shells were evaluated using a rigorous statistical approach, details of which may be found elsewhere [1, 20].

5. EXAFS results

5.1. Si edge EXAFS

k^3 weighted Si K-edge EXAFS functions and radial distribution functions (RDFs) (obtained by Fourier transformation using a Gaussian window to minimise truncation effects) are shown in fig. 3. Over the composition range studied ($0 < x < 0.18$) the phase and amplitude of the EXAFS signal remains approximately constant suggesting that the structure is dominated by the a-Si TRN. The RDFs all show the single peak at $R = 2.35$ Å characteristic of a-Si. There is little evidence apparent in the RDFs for the existence of Si–Sn correlations except for a small shoulder that is present on the high R side of the main RDF peak for the sample with $x = 0.18$.

Fitting of the theoretical EXAFS functions (results shown in table 1) to the data supports the above qualitative assertions. The Si edge data for the samples with x less than 0.07 are best interpreted in terms of a single shell of approximately 4 Si atoms at a distance of 2.35 Å. The Si–Si co-ordination of the sample with $x = 0.09$ appears to have decreased, although there is

Table 1
Structural parameters obtained from Si K-edge EXAFS results.

x	E_0 (eV)	VPI (eV)	N_{Si-Si} ± 0.8	R_{Si-Si} (Å) ± 0.01	A_{Si-Si} (Å^2) ± 0.002	N_{Si-Sn} ± 0.5	R_{Si-Sn} (Å) ± 0.02	A_{Si-Sn} (Å^2) ± 0.005
0.00	2.82	−3.31	4.1	2.34	0.006			
0.02	4.34	−2.82	4.0	2.34	0.006			
0.04	1.73	−4.21	4.2	2.35	0.005			
0.05	1.84	−4.17	4.3	2.35	0.005			
0.06	1.63	−4.29	4.0	2.35	0.005			
0.07	1.12	−4.12	3.8	2.35	0.004			
0.09	3.78	−3.91	3.1	2.34	0.004			
0.18	3.75	−3.41	2.9	2.35	0.004	0.6	2.61	0.015

little evidence to indicate Si–Sn correlations. However, the sample with $x = 0.18$ begins to show the presence of Sn atoms at a distance of 2.61 Å together with Si atoms at 2.35 Å, the total co-ordination number of 4 is retained. The lack of evidence for Si–Sn correlations ($x < 0.09$) in the Si edge EXAFS results is not surprising if we consider the fact that the results represent a structural average performed over the whole sample. For low levels of doping, assuming Sn atoms enter the structure in a random manner, the structure will continue to be dominated by Si–Si interactions. For a mechanism in which Sn atoms substitute randomly for Si atoms in the TRN it is necessary that there is 25 at% Sn for each Si atom to be bonded to a single Sn atom and 3 Si atoms. In this type of process the Si atoms retain fourfold co-ordination with the Si–

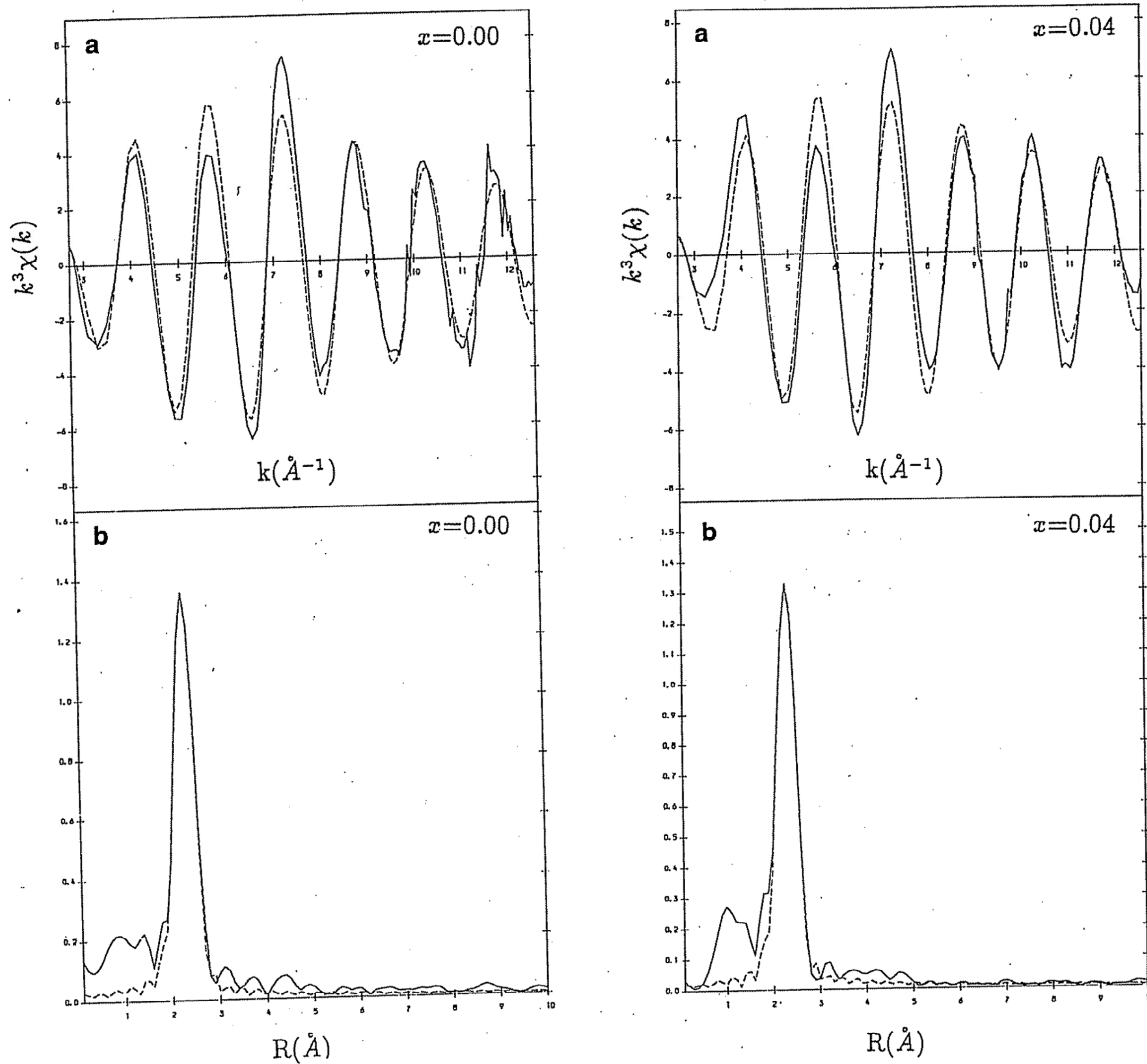

Fig. 3. (a) k^3 weighted Si K-edge EXAFS spectra and (b) radial distribution functions obtained by Fourier transformation. The solid curves are the experimental data and the dashed curves represent the best theoretical fits.

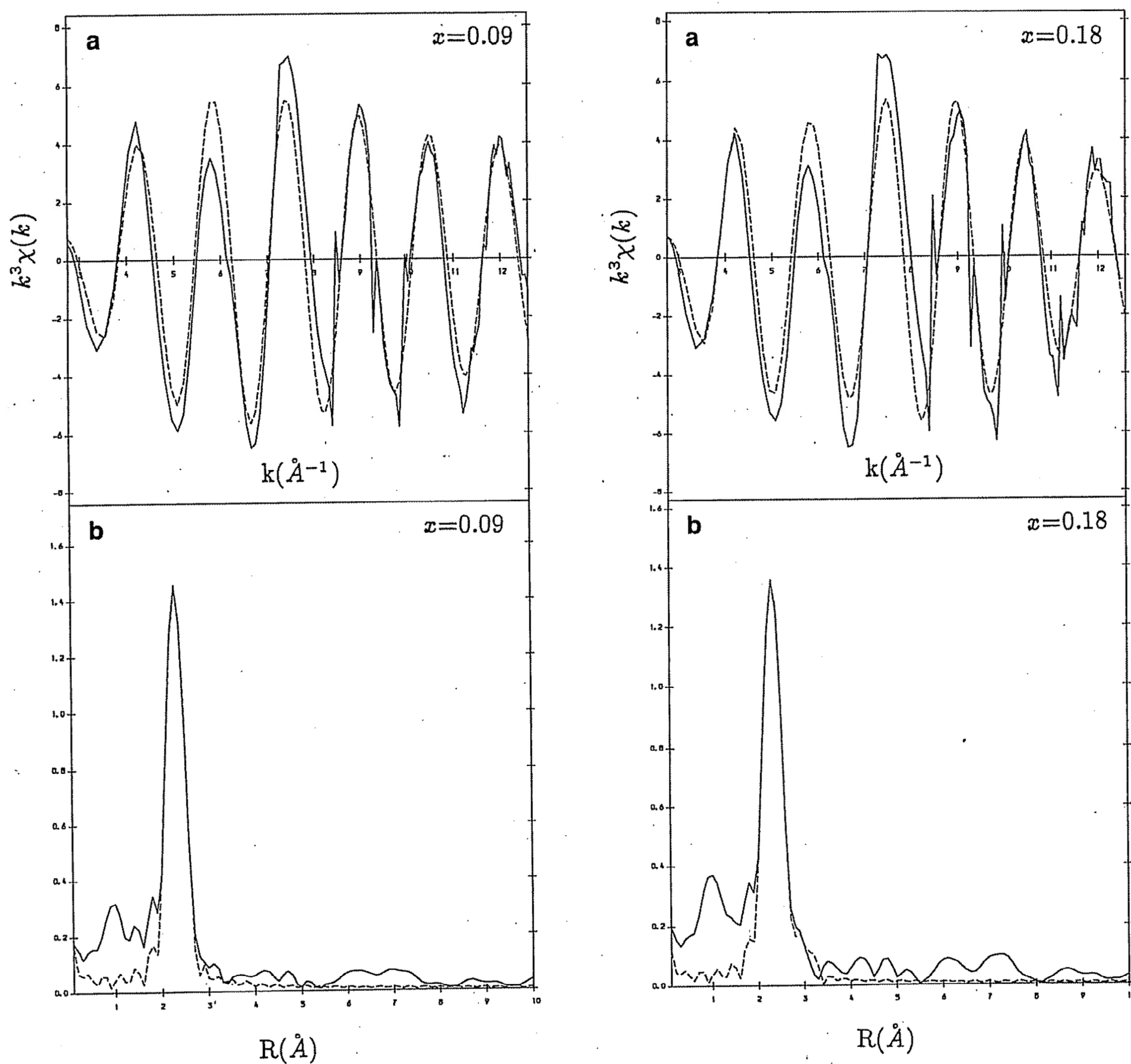

Fig. 3. (cont.).

Si partial co-ordination decreasing while the Si–Sn co-ordination increases. The Si edge EXAFS results may be used to support tentatively a substitution type mechanism for incorporating Sn atoms into a-Si:H.

5.2. Sn edge EXAFS

k^2 weighted EXAFS functions and RDFs obtained from the Sn K-edge experiments are shown in fig. 4. k^2 was used as a weighting factor rather than the more usual k^3 for the Sn K-edge to prevent exaggeration of the statistical errors present at higher energies. The structural parameters obtained in the fitting procedure are shown in table 2. Unfortunately, due to the aforementioned problems with the monochromator, the Sn edge spectra were noisy and had only a short useful energy range. This resulted in difficult background subtractions and very noisy RDFs,

especially at low real space distances. However, it is possible to distinguish between real and spurious peaks in the RDF by changing the range over which the Fourier transform is performed. The base peak observed at ~ 1.0 Å in some of the RDFs is an artefact of these background problems and obscures the peak due to atomic EXAFS at $R = 1.5$ Å in most cases. Since none of the spectra were Fourier filtered, this noise results in large errors in the parameters obtained from the best fits. However, the EXAFS spectra do not vary to within the experimental error across the composition range studied and the results, shown in table 2, suggest that over the whole composition range studied ($0 < x < 0.13$) Sn atoms are tetrahedrally coordinated to Si atoms. The Si–Sn interatomic distance suggested by the Sn edge results

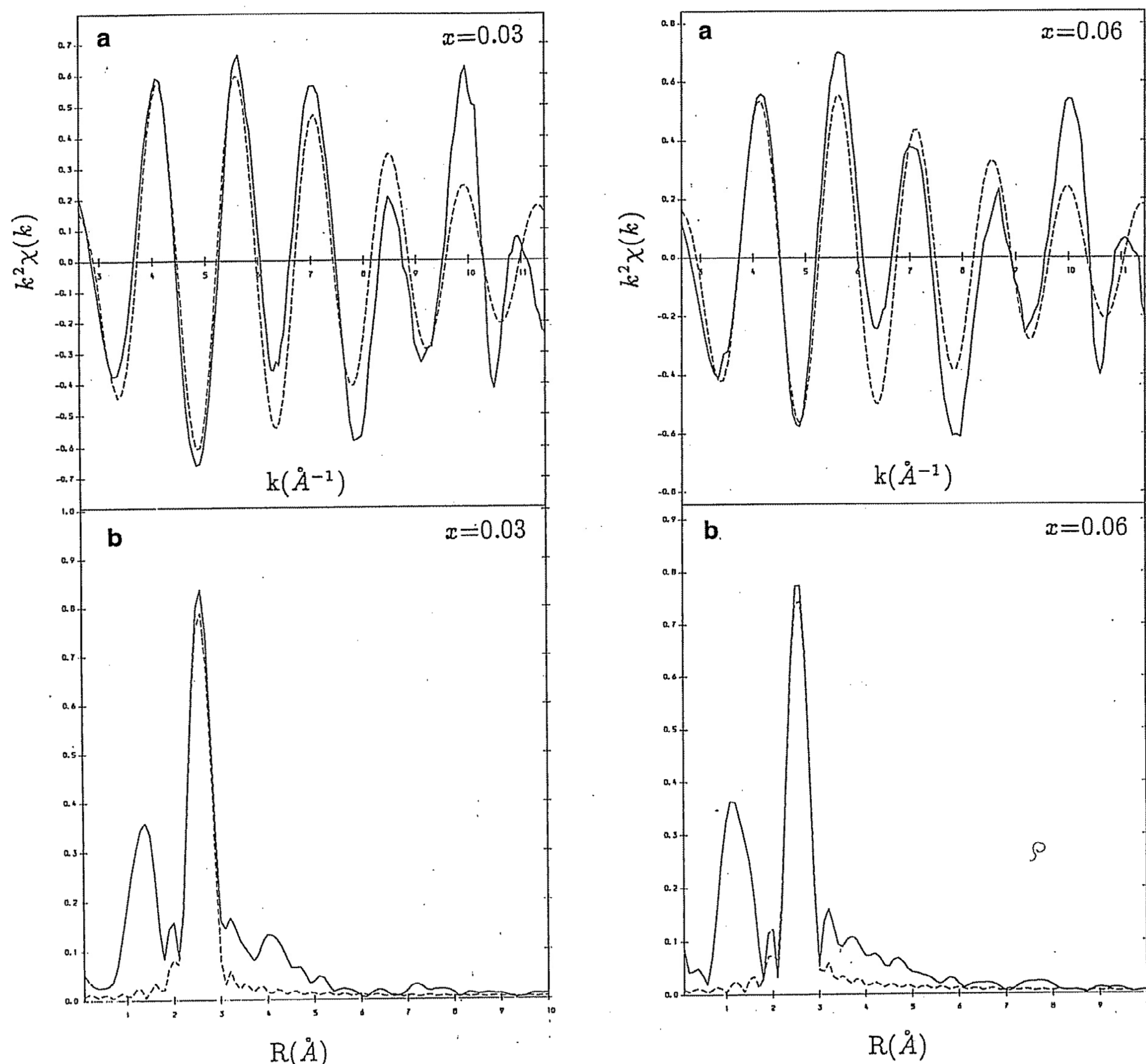

Fig. 4. (a) k^2 weighted Sn K-edge EXAFS spectra and (b) radial distribution functions obtained by Fourier transformation. The solid curves are the experimental data and the dashed curves represent the best theoretical fits.

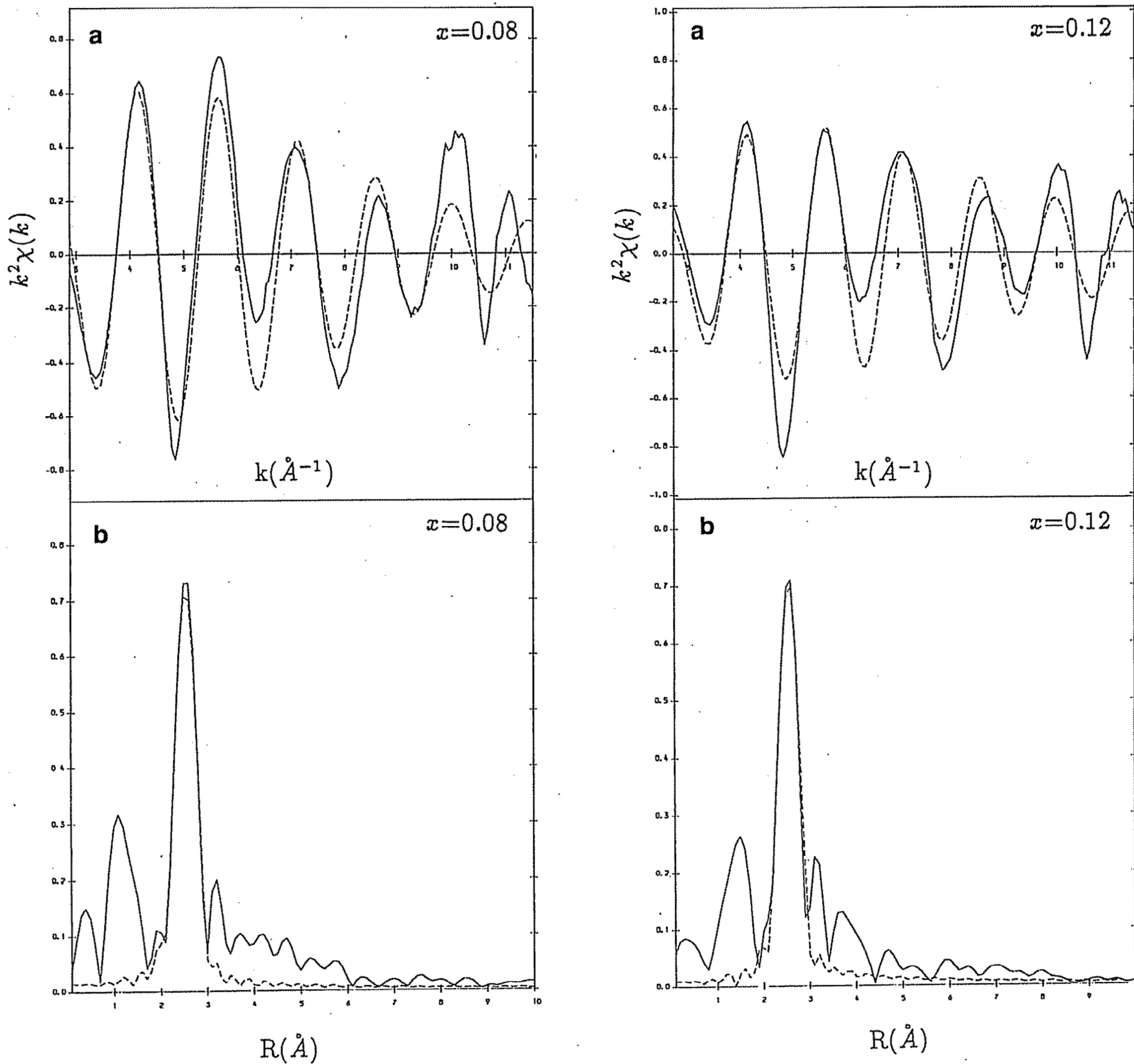

Fig. 4. (cont.).

(2.59 Å) agrees with that refined from the Si edge data for the sample with $x = 0.18$.

There is no evidence for a large contribution to the EXAFS from Sn–Sn correlations, although smaller contributions may be obscured by the poor quality of the Sn-edge data. As Sn scatters electrons much more strongly than Si, because of its much greater atomic number, the presence of sizeable clusters of Sn would be expected to feature strongly in the EXAFS spectra. This is obviously not the case, so we may safely conclude that the Sn atoms do not form large clusters.

6. Discussion

EXAFS results on the a-$Si_{1-x}Sn_x$:H system indicate that Sn atoms are substitutionally incorporated into the host a-Si:H network in the

Table 2
Structural parameters obtained from Sn K-edge EXAFS results. AFAC = 0.55.

x	E_0 (eV)	VPI (eV)	N_{Sn-Si} ± 1.5	R_{Sn-Si} (Å) ± 0.03	A_{Sn-Si} (Å^2) ± 0.008
0.02	0.00	−5.05	3.3	2.60	0.008
0.03	1.24	−5.00	4.2	2.59	0.008
0.04	2.55	−4.89	3.5	2.60	0.009
0.05	4.62	−3.46	3.3	2.61	0.007
0.06	4.38	−4.31	4.2	2.59	0.007
0.07	1.42	−4.14	3.6	2.59	0.005
0.08	6.46	−4.01	4.7	2.59	0.009
0.12	3.16	−5.45	3.9	2.60	0.008

composition range $0 < x < 0.18$. This is in agreement with the preferential tetrahedral coordination of Si atoms to each Sn atom observed by Vergnat et al. [9] in co-evaporated samples. No significant contribution from Sn–Sn correlations was observed in this low Sn concentration range. The lack of β-Sn crystallites corroborates the fact that a transition to metallic conduction was not observed by conductivity measurements. At least some of the Sn atoms would need to be incorporated in a metallic form for such an MIT to occur. The formation of β-Sn clusters has been observed by others to begin anywhere between 22 at% Sn [5] and 55 at% Sn [9]. Furthermore, there is no evidence for the formation of silicide-like regions of the form observed in other systems [1, 2]. Rather, the system appears to be completely homogeneous and the Si–Sn interatomic distances returned by the fits agree within errors with that suggested by a naive addition of the Si (1.18 Å) and Sn (1.40 Å) covalent atomic radii.

The lack of di- or tri-valently bonded Sn appears to be supported by the IR results where no Sn–H bonds were observed. Since conductivity measurements performed on these samples suggest an extended to localized state conduction transition (explained by the non-tetrahedral incorporation of Sn) at ~3 at% in agreement with others [3, 6–8], there appears to be some contradiction between results. However, the optical result has already provided the possible explanation that in the absence of sufficient H_2 to saturate all dangling bonds in the system, hydrogen will preferentially bond to the Si sites. Furthermore, other workers [7] have suggested that only a small percentage of the Sn atoms needs to be incorporated in a nontetrahedral fashion to cause the transition; the majority of the remaining Sn being incorporated substitutionally. If this is the case, then the average structure determined by EXAFS is unlikely to observe this small proportion.

7. Conclusions

Small concentrations of Sn atoms incorporated into a-Si:H by sputtering substitute for Si atoms in the TRN. Si atoms retain their fourfold coordination and Sn atoms also have four nearest neighbours. Si–Si and Si–Sn bond lengths are those expected for a covalently bonded system. Electrical conductivity measurements indicate the possibility of the incorporation of a very small amount of Sn in non-tetrahedral site causing a transition from extended to localized state conduction at ~3 at% Sn. In contrast to other amorphous semiconductor–metal alloys there is no evidence to suggest a locally modified structure (other than by the replacement of Si atoms by Sn atoms) and there appears to be no substantial clustering of Sn atoms.

Acknowledgements

The authors would like to thank members of the Physics Departments at the Universities of Kent and Leicester for the use of their equip-

ment and for discussions, especially E.A. Davis and S.J. Gurman. Thanks are also due to the staff of Daresbury Laboratory, particularly W. Myring, for assistance in performing experiments, and to C. Jeynes for his Rutherford backscattering analysis at SERC's facility at the University of Surrey. This work is supported by the SERC, and AME acknowledges receipt of a studentship from the University of Kent.

References

[1] A.M. Edwards, M.C. Fairbanks, R.J. Newport, S.J. Gurman and E.A. Davis, J. Non-Cryst. Sol. 113 (1989) 41.
[2] J.B. Kortright and A. Bienenstock, Phys. Rev. B 37 (1988) 2979.
[3] G.N. Parsons, J.W. Cook, Jr., G. Lucovsky, S.Y. Lin and M.J. Mantini, J. Vac. Sci. Technol. A 4 (1986) 470.
[4] A. Mohamedi, M.L. Theye, M. Vergnat, G. Marchal and M. Piecuch, Phys. Rev. B 39 (1989) 3711.
[5] D.L. Williamson, R.C. Kerns and S.K. Deb, J. Appl. Phys. 55 (1984) 2816.
[6] D. Girginoudi, N. Georgoulas and A. Thanailakis, J. Appl. Phys. 66 (1989) 354.
[7] A.H. Mahan, D.L. Williamson and A. Madan, Appl. Phys. Lett. 44 (1984) 220.
[8] B. von Roedern, A.H. Mahan, R. Könenkamp, D.L. Williamson, A. Sanchez and A. Madan, J. Non-Cryst. Sol. 66 (1984) 13.
[9] M. Vergnat, M. Piecuch, G. Marchal and M. Gerl, Phil. Mag. B 51 (1985) 327.
[10] D.L. Williamson and S.K. Deb, J. Appl. Phys. 54 (1983) 2588.
[11] Zhang Fangqing, He Deyan and Chen Guanghua, Chin. Phys. Lett. 3 (1986) 245.
[12] J. Vossen and W. Kern, eds., Thin Film Processes (Academic Press, London, 1978).
[13] M.I. Manssor and E.A. Davis, private communication (1988).
[14] N. Maloufi, A. Audouard, M. Piecuch, M. Vergnat, G. Marchal and M. Gerl, Phys. Rev. B 37 (1988) 8867.
[15] W.T. Elan, J.P. Kirkland, R.A. Neiser and P.D. Wolf, Phys. Rev. B 38 (1988) 26.
[16] Synchrotron Radiation, Appendix to the Daresbury Laboratory Annual Report (1987/1988).
[17] C. Morrel, J.T.M. Baines, J.C. Campbell, G.P. Diakun, B.R Dobson, G.N. Greaves and S.S. Hasnain, Daresbury Laboratory EXAFS Users Manual (1989).
[18] S.J. Gurman, N. Binsted and I. Ross, J. Phys. C 17 (1984) 143.
[19] N. Binsted, S.J. Gurman and J.C. Campbell, SERC Daresbury Laboratory EXCURV88 Program (1988).
[20] R.W. Joyner, K.J. Martin and P. Meehan, J. Phys. C 20 (1987) 4005.